



Additive Manufacturing of Bio-Inspired Microstructures for Bone Tissue Engineering

N. Top¹ · H. Gökçe¹ · I. Şahin¹

Received: 29 September 2022 / Accepted: 30 January 2023 / Published online: 14 February 2023
© The Society for Experimental Mechanics, Inc 2023

Abstract

Bone Tissue Engineering (BTE) focuses on restoring tissues that have lost their function due to disease or trauma. Porous artificial scaffolds are used in order to restore the structural functions of bone tissues. In recent years, Additive Manufacturing (AM) technologies that can be integrated into Computer-Aided Design (CAD) software have shown great potential in this field. The use of AM technologies in the production of bone scaffolds made it possible to construct structures with appropriate mechanical properties and different configurations. In this study, artificial bone scaffolds designed using bio-inspired geometries and Computer-Aided System for Tissue Scaffolds (CASTS) library were printed by Fused Deposition Modeling (FDM) method using Acrylonitrile Butadiene Styrene (ABS) and Polylactic Acid (PLA) materials. The aim of this study is to investigate the effects of bone scaffolds created with bio-inspired microstructures on dimensional accuracy, weight, mechanical performance, structural strength, porosity and pore size. According to the test results, PLA printed scaffolds have better results than ABS printed scaffolds in terms of dimensional accuracy, porosity, pore diameter and weight. Among the PLA-printed scaffolds, the high pore diameter of the scutoid geometry resulted in low mechanical strength. In terms of porosity, the icosahedron geometry gave better results than the cubic structure. Therefore, PLA-printed icosahedron geometry can be considered as the most suitable scaffold type for bone tissue regeneration.

Keywords Bone tissue engineering · Additive manufacturing · Bone scaffold design · Bio-inspired structures

Abbreviations

ABS	Acrylonitrile butadiene styrene
AM	Additive manufacturing
β-TCP	Beta tricalcium phosphate
BG	BioGlass
CT	Computed tomography
CAD	Computer-aided design
CASTS	Computer-aided system for tissue scaffolds
ECM	Extracellular matrix
FDM	Fusion deposition modeling
HA	Hydroxyapatite
MRI	Magnetic resonance imaging
ME	Material extrusion
PCL	Polycaprolactone
PGA	Polyglycolic acid
PLA	Polylactic acid
3D	Three dimensional

BTE	Bone tissue engineering
TCP	Tricalcium phosphate

Introduction

The healing ability of the bone is insufficient in the regeneration of bone defects caused by cancer, trauma, fracture, infection and accident [1, 2]. In such challenging cases, tissue transplantation is performed in the same individual (autograft) or bone tissue from a deceased individual (allograft) is used [3, 4]. Bone Tissue Engineering (BTE), which is a multidisciplinary approach related to fields such as mechanical engineering, genetics, clinical medicine, materials science, biology, includes studies on the regeneration of damaged bone [5]. BTE aims to restore and replace lost tissue functions by overcoming difficulties and limitations in the treatment process. In bone regeneration, properties of the Extracellular Matrix (ECM) such as mechanical support, cellular activity, and protein production through biochemical and mechanical interactions are mimicked [6, 7].

✉ H. Gökçe
harungokce@yahoo.ca

¹ Technology Faculty, Industrial Design Engineering Department, Gazi University, Ankara, Turkey



Bone scaffolds task as carriers for growing bone tissue, cartilage, skin, blood vessels, nerves and muscles [8]. Biocompatibility and biodegradability are important considerations to obtain bone scaffolds with high mechanical strength and porosity [9, 10]. Hierarchically increasing porous micro and nanostructures from cancellous to cortical bone determine the mechanical strength of the bone. The interconnected porous scaffolds, which are important for the growth of bone tissue, are responsible for the removal of waste materials, vascularization and cell growth [11, 12]. Although high porosity is important for the diffusion of nutrients, excessive porosity reduces the mechanical strength of the scaffold and causes it to be damaged under the force applied by the growing cells [13]. Therefore, Gregor et al. [14] stated that 90% and above porosity is not necessary.

Conventional methods such as salt leaching, gas foaming, solvent casting, phase separation, freeze drying are used in the production of artificial bone scaffolds for TE. However, it is very difficult to control pore geometry, pore size and distribution of the pores with them. Besides, these methods characterized by poor repeatability [15]. The limitations of conventional methods lead to the use of popular production methods such as Additive Manufacturing (AM) in BTE applications. AM provides high accuracy, repeatability, controlled porosity and rich material diversity, as well as making it possible to produce complex microstructures with the advantages it offers in the control of scaffolds structures [16]. The production of customized, free-form scaffolds in various stiffness levels is possible with AM that can control pore size and pore shape directly from Computer Aided Design (CAD file data without the need for a die [17–19].

The necessary data for the Three-Dimensional (3D) scaffold models to be created in CAD software are obtained by medical imaging techniques such as Computed Tomography (CT) and Magnetic Resonance Imaging (MRI) [20]. Different methods such as CAD-based design, image-based design, implicit surface design, topology optimization, and space-filling curves are used in the design of bone scaffolds that affect cell behavior and mechanical properties [21]. In addition to these methods, biomimetic-based approaches are used to obtain the closest geometry to the bone structure in the bone scaffold design [22, 23].

In the literature, these studies mostly focused on the image-based design method to imitate the structure of natural bone. An analytical image of the damaged area is obtained with medical imaging methods such as CT and MR and combined with the internal pore architecture created on a CAD platform with Boolean operations and the scaffold image is created [24, 25]. On the other hand, by using bio-inspired cellular units in the CASTS system, scaffolding architects closest to the natural bone structure can be obtained directly. In this approach, bio-inspired cellular structures are used, inspired by microorganisms existing in

nature [21]. It is aimed to design high performance cellular structures inspired by structures existing in nature such as honeycomb, shark skin denticles, turtle rib and wheat awn [26–28]. Ghazlan et al. [29] developed a new bio-inspired cellular structure mimicking the thin-walled structure of trabecular bone. The resulting structure was compared with conventional hexagonal and re-entrant designs. Another study by Ghazlan et al. [30] developed a new cellular unit inspired by the complex cellular structure of trabecular bone.

Therefore, the main objective in the design of artificial bone scaffold is to obtain the geometry closest to the structure of the nature bone. It is extremely difficult or impossible to produce scaffolds designed in computer environment with conventional manufacturing methods [2]. With the integration of CAD software into AM technologies, pore shape, pore size and porosity can be controlled during the pre-production design phase [31]. In CAD based design, which is one of the most widely used methods in the scaffolding design process, porous scaffolds are obtained by periodically increasing cellular units such as cylinders, cubes and prisms [32]. In the nature bone structure, different from these primitive structures, there are some irregular and gradient pores array unit cell geometries [33, 34]. Cellular unit design has a direct impact on the mechanical performance of porous scaffolds. For this reason, there are studies focusing on cellular structure design in the literature [35–37].

Different AM technologies may need to be used for 3D printing of different biomaterials that affect the performance of artificial bone scaffolds [2]. Biopolymers, bioceramics, biocomposites and biometallic materials are used to obtain the scaffold structure closest to natural bone [38]. Polymeric and metallic materials have long been used as load-bearing biomaterials [39]. Metallic materials are more suitable for load-bearing areas such as the spine, pelvis, and chest [40–42]. Polymeric materials are used in dental implants, prostheses and anatomical models, as well as in bone regeneration due to their biocompatible and biodegradable properties [43]. Bioceramics are mostly used as fillers in bone defects [43].

Artificial bone scaffolds are mostly produced from biodegradable natural or synthetic polymers so that they can be fully resorbed and perform the mechanical function until the defected tissue is regenerated [15]. Among AM technologies, there are three main methods using synthetic polymers: extrusion-based 3D printing, laser/light assisted 3D printing, and inkjet 3D printing [44, 45]. Material extrusion (ME) is the most widely used 3D printing method in synthetic polymer applications. Besides synthetic polymers, bioactive ceramics and composites are widely used in ME [46]. Synthetic polymers are preferred in BTE studies due to their controlled degradation rates [47]. In addition, synthetic polymers can be produced in complex shapes, at low cost, in large quantities, and have a longer shelf life [46]. Among the most used synthetic polymers in bone scaffold

studies, Polylactic Acid (PLA) [48–51], Acrylonitrile Butadiene Styrene (ABS) [52–54], Polycaprolactone (PCL) [55, 56] and Polyglycolic Acid (PGA). Bioactive Ceramics such as Hydroxyapatite (HA), Tricalcium Phosphate (TCP), Beta Tricalcium Phosphate (β -TCP) and BioGlass (BG) chemically imitate bone, as they have high compressive strength and low ductility [57]. Because of these properties, to increase the biocompatibility of polymer bone scaffolds, either polymer scaffolds are coated with these materials [58–61] or biocompatible polymer-ceramic composites they are created and used [62–67].

While the bioactivity of the materials used in the production of artificial bone scaffolds is important to support bone attachment and osteocompatibility, their biodegradability is necessary for the growth of bone tissue [68]. Poly(L-lactide), one of the polymers that is well biodegradable and has high biocompatibility [69, 70], has been approved by the United States Food and Drug Administration for its use in tissue engineering [71]. Thus, PLA is a biocompatible, biodegradable, non-toxic, and resorbable aliphatic polyester characterized by its high melting temperature (160 °C) [72]. In addition to these properties, it is used in biomedical scaffold studies due to its non-inflammatory properties against the human body [72]. Besides, due to successful biodegradability and biocompatibility, PLA is widely used in BTE applications [73, 74]. ABS materials are also a subject of research as a potential material in bone scaffold applications. ABS has advantages in terms of dimensional stability, tensile strength, surface hardness and chemical properties. ABS used in 3D printing processes in various fields are also preferred in BTE applications [75, 76]. However, there are limited studies comparing ABS and PLA in the production of porous scaffolds with AM. Krishna et al. [51] compared porous scaffolds produced with ABS and PLA materials in terms of mechanical properties and porosity. Ariffin et al. [52] compared the performance of circular and rectangular scaffolds by measuring the compressive strength and elastic modulus of porous ABS scaffolds produced by 3D printing. Rosenzweig et al. [54] compared ABS and PLA scaffolds for cell ingrowth, viability, and tissue generation.

In the literature, there are some studies in which ABS and PLA materials are prepared jointly. It is stated that ABS/PLA composites show poor mechanical properties [77]. It is seen that Graphene Nanocomposite structures are used in PLA/ABS composite structures to strengthen the weak mechanical properties of PLA/ABS composites [78]. There are also studies using epoxy made of Styrene Acrylonitrile and Glycidyl Methacrylate (SAN-GMA) to increase the mechanical properties of PLA/ABS composites. Studies have shown that the SAN-GMA epoxy mixture improves the mechanical properties of PLA/ABS composites [79, 80].

Pore size, porosity and mechanical properties affect the performance of bone scaffolds [21]. High porosity

increases the surface area per unit volume, while pore size is important for cell migration and infiltration [11]. Additionally, interconnected pores, are directly effective in cell growth, nutrient delivery, vascularization, and removal of waste materials [21]. There are studies in the literature investigating the porosity and mechanical properties of CAD-based artificial bone scaffold designs [2, 81–83]. The design of the scaffold affects cell behavior and the mechanical properties of bone [84]. On the other hand, there are studies in the literature that perform biological experiments as well as mechanical tests to determine the effect of pores on bone tissue regeneration [85–87]. The results of biological experiments show that the produced scaffolds have significant potential for bone repair.

In this study, scaffold designs developed using bio-inspired cellular units were compared in terms of dimensional accuracy, weight, porosity, pore size and mechanical properties. The porosity and mechanical properties of the scaffolds designed in CAD software were compared with PLA and ABS-P430 printed scaffolds and the dimensional accuracy of extrusion-based AM technologies was evaluated. The importance of microscopic evaluation of artificial bone scaffolds is to determine the effect of different cellular unit designs on porosity. The focus of the study is to determine the effect of bio-inspired cellular units, used for the first time in the literature, on bone tissue regeneration. Additionally, due to the limited BTE study using ABS-P430 [53, 88], the results of the study include the findings of 3D-printed artificial bone scaffolds to be produced using ABS-P430.

The following sections of this paper are organized as follows. Section "Materials and Methods" includes research methodology. In Section "Results and Discussions", results and findings are presented. Finally, conclusions are presented in Section "Conclusions".

Materials and Methods

In this study, three different unit cells were designed and produced using the FDM method, utilizing the unique design freedom provided by AM technologies. The measurement accuracy of 3D printed PLA and ABS scaffolds was tested and compared in terms of mechanical strength.

Materials and 3D Printers

The 3D bone scaffolds designed in the study were produced with PLA and ABS. The density of PLA is 1.24 g/cm³, tensile strength 110 MPa, tensile modulus 3.309 GPa, melting point 160 °C and filament diameter 2.85 mm. The production of PLA scaffolds was carried out with the Ultimaker 3 (Ultimaker, Netherlands) machine without using any support material. The printing parameters have

0.4 mm nozzle diameter, are set to be nozzle temperature 180–280 °C, build plate temperature 100 °C and layer thickness 200 microns. During the printing of PLA scaffolds, the nozzle temperature was determined to be 210 °C and the build plate temperature to 60 °C.

The production of ABS scaffolds was carried out with the Stratasys uPrint® SE (Stratasys, Israel) machine using SR-30XL soluble support and ABSPlus-P430 filament. The density of ABS filament used in printing is 1.04 g/cm³, tensile strength 31 MPa, tensile modulus 2.2 GPa, melting point 210 °C, filament diameter 1.75 mm and elongation at break is 6%. The nozzle diameter of Uprint SE Plus, which has double nozzles, is 0.4 mm, nozzle temperature 180–280 °C, build plate temperature 100 °C, layer thickness 254 micron and build size 203 × 203 × 152 mm. The printing temperature to produce ABS scaffolds cannot be determined by the user due to the closed system feature of the printer. The printer automatically determines the printing temperature in the range of 180–280 °C. The ambient temperature is similarly set at 100 °C by the printer.

Scaffold Design

CAD based design of artificial bone scaffolds uses bottom-up and top-down design approaches. In the unit cell design method used in bottom-up approach, 3D scaffold architectures are obtained by creating periodically repeating geometric units [89]. Thus, the desired change can be achieved on the mechanical properties of the scaffold. The design of the scaffold structure affects the mechanical properties and cell behavior of the bone [84]. For this reason, this process must be managed properly.

With the CASTS library used in the unit cell design, by subjecting standard solid units such as cubes, hexagons, spheres and cylinders, which are ready to use in CAD programs, to boolean operations such as extraction, intersection and union, simple scaffold geometries can be obtained periodically [90]. The CASTS aims to automate the scaffolding design process while shortening the design process. The use of bio-inspired designs in this system is a good alternative to improve the mechanical performance of bone scaffolds, enrich the scaffold library, and increase the stability of the structure and tissue energy efficiency [89].

In the study, three different geometries were used in the design of scaffold structures. Two of them are bio-inspired, the other unit cell is the cubic structure in the CASTS library. The scutoid form, inspired by the way cells in the epithelial tissue pack together [91], is one of the bio-inspired cellular units used in the study. Using this form, scaffolds with high porosity and optimum strength can be created by mimicking tissue-forming behavior of nature in artificial bone and organ production. Another geometric form used in the study is icosahedron, which is considered a bio-inspired

geometry because it reflects the form of many virus shells. The unit cells were designed at the same scale using Catia software. Thus, the bone scaffold design process consists of three main process steps:

- Wireframe design of unit cells,
- Creation of solid models from wireframes,
- Creation of bone scaffold structure by periodically reproducing unit cells in X, Y and Z axes.

Therefore, to obtain the 3D scaffold structure, the scutoid was first brought together in pairs (the hexagonal and pentagonal surfaces should contact each other), then these binary structures were increased periodically (Fig. 1).

The dimensions of the designed unit cells are equal (2 mm), the heights differ due to the structure of the geometries. The height of the scutoid is 4 mm, the height of the icosahedron and cubic geometries is 2 mm. Strut diameters of all unit cells were determined as 400 μm. Bone scaffold structures were obtained with the periodic increase of unit cells along the X, Y and Z axes (Fig. 2). In order to compare the performance of unit cells equally in terms of porosity, mechanical and structural strength, scaffold architectures of equal dimensions (20 × 20 × 20 mm) were created.

Porosity and Pore Size

Scaffold vascularization is very important in the implantation processes of unit cells and structural scaffolds. High porosity and large pores increase postoperative vascularization and osseointegration of the implant [92]. Porosity, pore size and mechanical strength affect scaffold performance [12]. The most important property for the continued growth of bone tissue is the interconnected porosity. Interconnected pores provide waste material removal, vascularization, cell growth and nutrient delivery to the inner part of the scaffold. High porosity is also important to increase the surface area per unit volume [11, 12]. For the formation of an ideal bone structure, 3D scaffolds must have high porosity and these pores must be well connected to each other. Spinal porosity is typically between 50 and 90% compared to total nominal volume [93]. High porosity is desirable as it provides higher tissue growth volume and nutrient transport efficiency. However, it is possible that the mechanical strength decreases as the porosity increases [94].

In order to determine the porosity ratio of the scaffold structures developed in this study, the bulk volumes (V_B) of the designed cellular units are calculated first (equation (1)). Then the volumes of the produced porous units are calculated (V_{sk}) (equation (2)). Porosity is calculated by equation (3) [50].

Fig. 1 From microstructure to macrostructure: scutoid unit cell

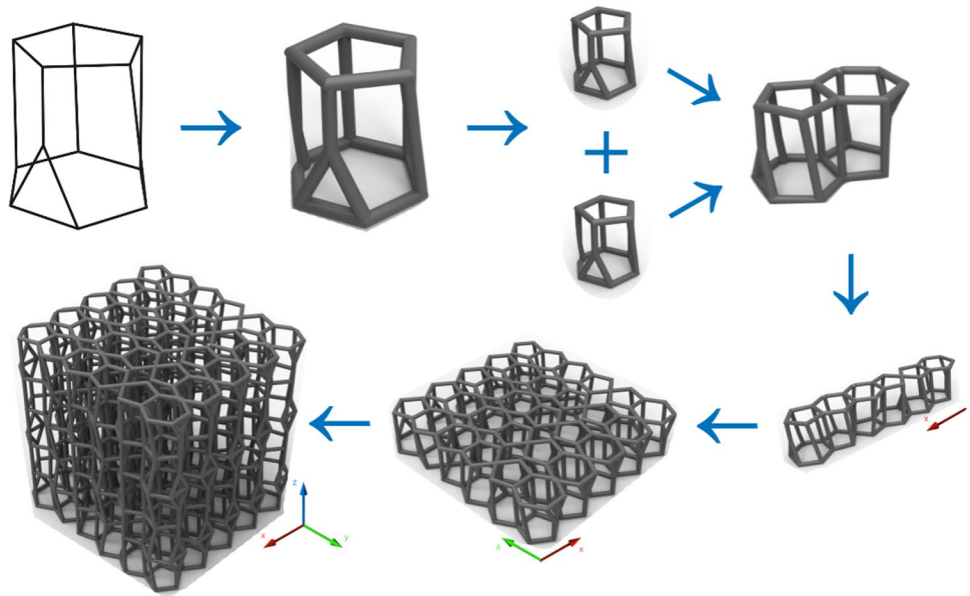


Fig. 2 Design of scaffold structures: (a) Scutoid, (b) Icosahedron, (c) Cubic ($L_s = 2\text{ mm}$, $S_d = 400\text{ }\mu\text{m}$, $L = 20\text{ mm}$, $H = 20\text{ mm}$)

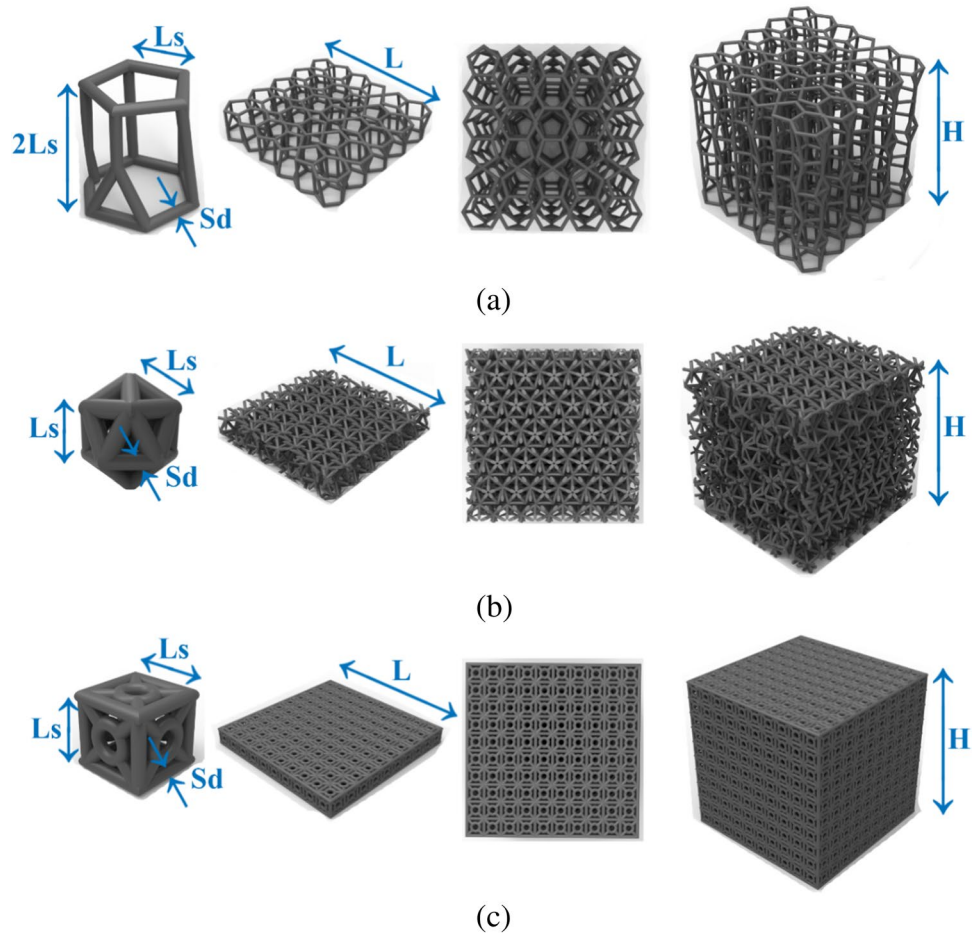
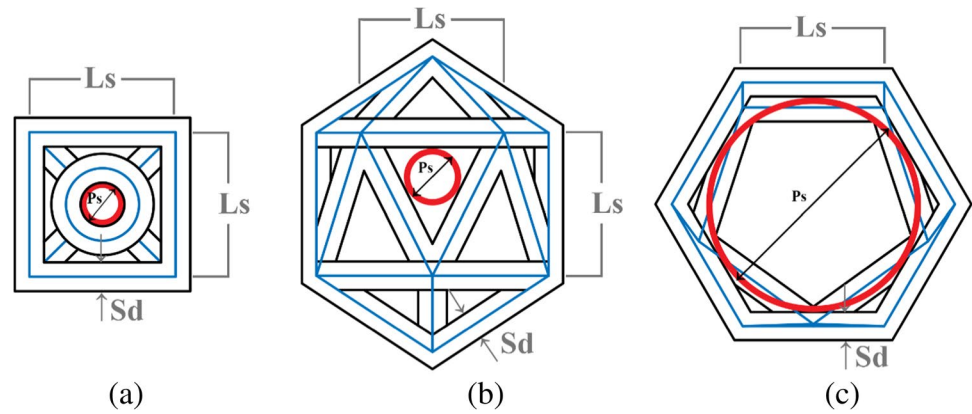


Fig. 3 Pore size identification of the cellular units: (a) Cubic, (b) Icosahedron, (c) Scutoid



$$V_B = W \times H \times L \quad (1)$$

where W, H and L are the width, height and length of the scaffold structure, respectively.

$$V_{sk} = \frac{m}{\rho_{mat}} \quad (2)$$

where m is the mass of the bone scaffold, it is the material density. The density (ρ_{mat}) is 1.24 g/cm³ for PLA material and 1.04 g/cm³ for ABS material.

$$Porosity[\%] = \frac{V_B - V_{sk}}{V_B} \times 100 \quad (3)$$

Different methods such as line intercept, maximal covering spheres and largest inscribed circle are used in pore size calculation [12, 95, 96]. Egan et al. [93] reported that pore size is based on the largest circular cross-section diameter (Fig. 3).

In the calculation of pore sizes shown in Fig. 3, equation (4) for cubic cellular unit, equation (5) for icosahedron and equation (6) for scutoid were used. Where P_s , L_s and S_d are pore size (mm), edge length of cellular unit (mm), strut diameter (mm), respectively.

$$P_s = [L_s(\sqrt{2} - 1)] - S_d \quad (4)$$

$$P_s = \frac{L_s}{\sqrt{3}} - S_d \quad (5)$$

$$P_s = L_s\sqrt{3} - S_d \quad (6)$$

Finite Element Analysis

3D model was created in CATIA. To determine the stress distribution on the scaffold for FEA studies was used by ANSYS. Firstly, a unit element is modeled as a wireframe

Table 1 FEA elements and nodes quantities

Geometry	Nodes	Elements	Connectivity
Cubic	423,743	1,174,776	TE4/Spider
Icosahedron	137,782	317,483	
Scutoid	71,453	196,482	

Table 2 Material mechanical properties

Material/Structure	Young's modulus (MPa)	Poisson's ratio
ABS P430	31	0.28
PLA	110	0.29

in 3D environment and then transformed into a combined solid model. The unit element, which was converted to a solid model in the CATIA, was cloned planarly with a length of min 25 mm. In the standard given for pressure tests in ASTM-D1621, it is stated that the dimensions should be at least 25 mm. Boundary condition was prepared in the same way as for the experimental compression test setup. Scaffold bottom surface are constrained in all directions as $DOF=0$. A load of 50 kN was applied to its upper surface with a rigid plate.

The mesh quality established for the FEM is of vital importance for the calculation result. Mesh sizes used in the scaffolds are given in Table 1. Besides, the modulus of elasticity and poisson rates of the materials used in FEA are given in Table 2.

Compression Test

20 × 20 × 20 mm test specimens were produced using ASTM D1621-00 standard in order to characterize the compression behavior of scaffold models in different geometries produced with ABS and PLA materials. Samples were tested at different compression rates

in order to infer the effects of compression speed on strength. Mechanical tests were performed with a computer controlled Schmadzu AG-I 250 kN pressing and drawing machine and the results were processed in a computer environment. In the compression test, 50kN load was applied to the models in vertical direction with a speed of 5 mm/min. The test setup is shown in Fig. 4.

Results and Discussions

In the results and discussions section, the effects of three different bone scaffold designs printed with PLA and ABS on dimensional accuracy, weight, porosity, pore size and mechanical strength are discussed comparatively.

Dimensional Accuracy

Bone scaffolds were produced with two different materials using the FDM method. PLA scaffolds were printed using the Ultimaker 3 printer, while ABS scaffolds were printed using uPrint® SE (Fig. 5). According to the printing results, PLA scaffolds have better surface quality than ABS scaffolds. The problem of dissolving the support material in ABS scaffolds has reduced the surface quality. On the other hand, PLA scaffolds were printed without the use of support material and are lighter than ABS scaffolds. Although the density of PLA is higher than ABS, the use of support material in ABS printing has increased the weight. The weights of the printed scaffolds were measured and compared with the CAD models (Table 3).

Fig. 4 Compression test setup

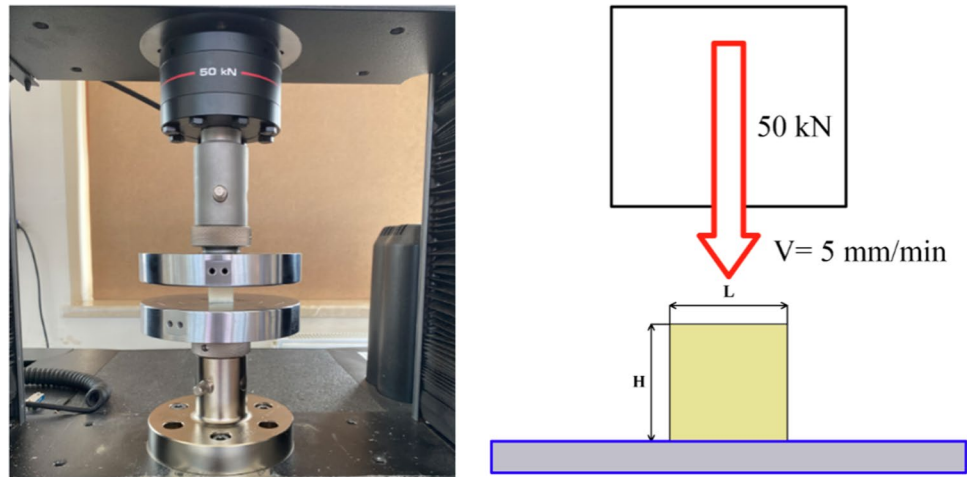


Fig. 5 Isometric and top view of scaffold structures

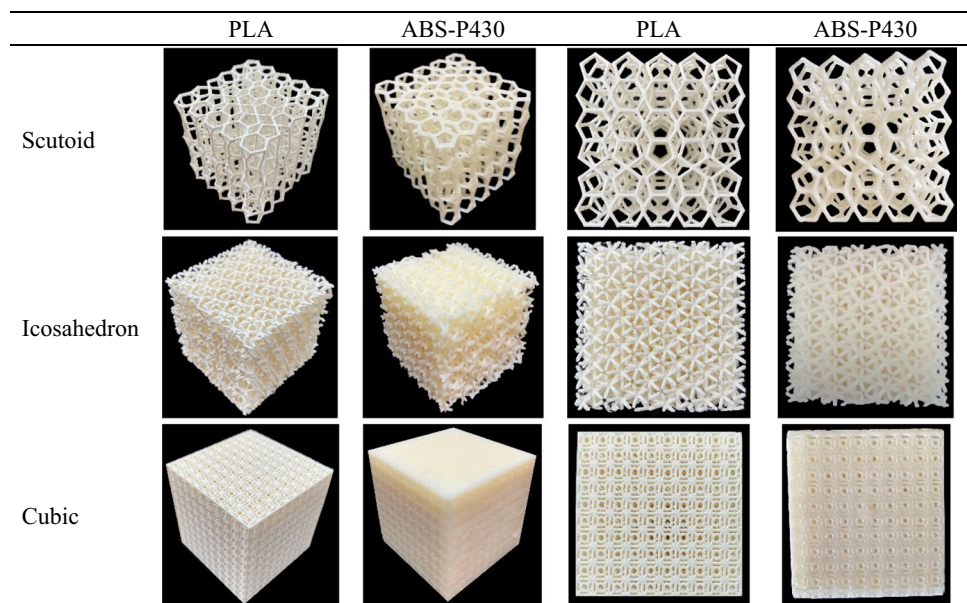
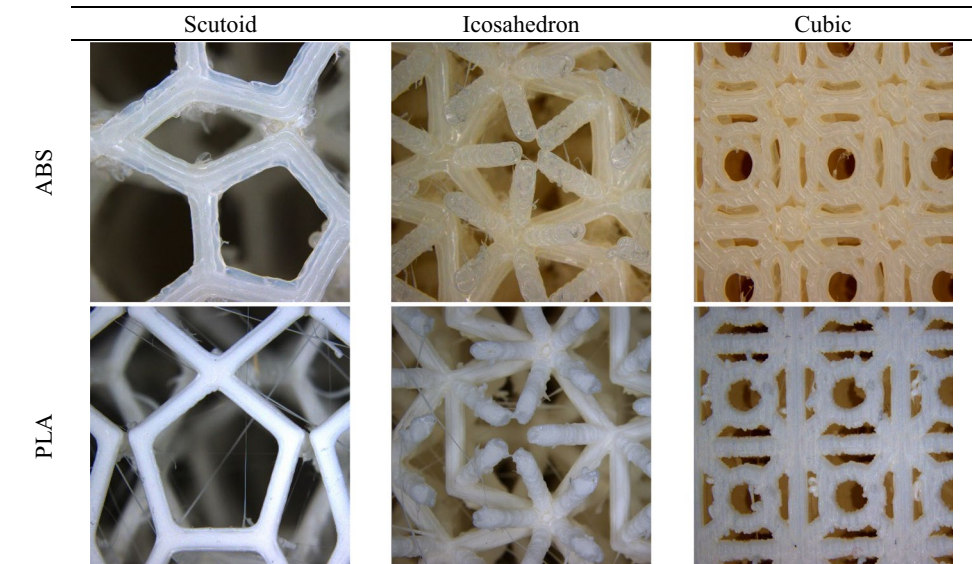


Table 3 Comparison of basic dimensions for scaffold models

Structures	CAD strut Ø (µm)		Printed strut Ø (µm)		CAD weight (gr)		Printed weight (gr)	
	PLA	ABS	PLA	ABS	PLA	ABS	PLA	ABS
	Scutoid	400		409	416	0.478	0.407	0.52
Icosahedron			411	418	1.562	1.295	1.574	1.79
Cubic			415	421	3.137	2.674	3.298	3.663

Fig. 6 Micro image of the scaffold structures

In order to determine the conformity of the printing results with the design expectations, the strut diameters and pore sizes of the printed scaffolds were measured with the Dino-Lite AM3113T Digital Microscope. According to the microscope images, it is seen that the support material is not sufficiently dissolved due to the low porosity of the cubic structure printed with ABS (Fig. 6). Therefore, these structures performed worse than PLA in porosity, internal pore and surface quality. Printing PLA scaffolds without support material has an effect on this result. In both PLA and ABS printed scaffolds, the design expectations are met due to the fact that the foot connections and scaffold geometries are close to the nominal dimensions. Scutoid and icosahedron structures printed with ABS are better than cubic structures in terms of geometry, porosity, strut connections and surface quality. Scutoid scaffolds printed with PLA have the best results in terms of surface quality, interconnectivity and porosity.

The measurement results of the printed scaffolds, whose strut diameters were measured with a digital microscope, were compared with the CAD model. The strut diameters of all scaffolds are 400 µm, and the scaffold models were designed in dimensions of 20 × 20 × 20 mm. The strut diameters of printed PLA scaffolds were measured as

405 µm for scutoid, 403 µm for icosahedron and 403 µm for cubic structure, while the strut diameters of ABS scaffolds were measured as 408 µm for scutoid, 406 µm for icosahedron and 405 µm for cubic structure (Table 3).

According to the results, PLA scaffolds are more consistent than ABS in terms of dimensional accuracy. The strut diameters of PLA printed structures deviate maximum 3.75% from the design diameter and ABS printed structures deviate maximum 5.25%. These deviation rates indicate that the printing was quite successful. The lowest deviation rates were seen in PLA printed icosahedron and cubic structures and ABS printed cubic geometry. These results show that both geometries have a uniform structure.

Porosity and Pore Sizes

In line with this study, the pore size and porosity of the scaffolds after 3D printing were determined and compared with CAD models (Table 4). According to the results, the scutoid has the highest porosity with 94.7% in PLA printed scaffolds. This is followed by icosahedron with 84.1% and cubic structures with 67.7%, respectively. The use of support materials in the printing of ABS scaffolds has reduced the porosity. On the other hand, in ABS printed

Table 4 Porosity ratios and pore sizes of the different structures

Structures	CAD porosity (%)	Printed porosity (%)		Deviation (%)		CAD pore size (µm)		Printed pore size (µm)		Deviation (%)	
		PLA	ABS	PLA	ABS	PLA	ABS	PLA	ABS	PLA	ABS
Scutoid	96.9	94.7	93.3	1.35	3.7	3060	3060	3025	3008	1.14	1.69
Icosahedron	90.2	84.1	78.4	6.76	13.08	756	756	722	697	4.49	7.8
Cubic	79.9	66.7	55.9	16.52	30.03	428	428	411	405	3.9	5.37

scaffolds, the structure with the lowest porosity is the cube with 55.9%, while the scutoid has the highest porosity rate with 93.3%. The porosities of the CAD models of the scaffold designs are 96.9% in the scutoid, 90.2% in the icosahedron and 79.9% in the cubic, respectively. When the deviations in design and printing porosity are examined, it is seen that PLA printed scaffolds have lower deviations. The results obtained demonstrate the success of additive manufacturing to control porosity.

The pore size of a bone scaffold is important parameter that affects the quantity and characteristics of new tissue formation [97, 98]. The pore size is an important parameter that affects the quantity and characteristics of new tissue formation. The pore sizes of 10–2250 µm were used in BTE studies [98]. Macro porous increase bone ingrowth by increasing permeability, while small pores are more suitable for soft tissue ingrowth [99]. Bragdon et al. [100] reported that mean pore size ≥ 200 µm and porosity $\geq 40\%$ were optimal for bone growth. Karageorgiou and Kaplan [97] suggested pore sizes > 300 mm due to increased new bone formation and the formation of capillaries. Ghayor and Weber [101] indicated the beneficial effects of pore sizes between 700–1200 µm. Abbasi et al. [99] reported that pore sizes between 100–600 mm allow better integration with the host bone tissue, subsequent vascularization and bone distribution. Roosa et al. [98] indicated that significant bone formation in 800 mm scaffolds.

Besides, there are studies that recommend pore sizes up to 500–1000 µm for cancellous bones [102] and for cortical bones up to 500 µm [8]. In this study, the pore sizes of PLA and ABS printed scaffolds varies between 411 and 3025 µm. The pore sizes of PLA printed cubic and icosahedron structures are 411 µm and 722 µm, respectively. In ABS printed scaffolds, the pore sizes were measured as 697 µm for the icosahedron and 405 µm for the cubic, respectively. Therefore, the results show that cubic and icosahedron structures can be used as scaffold geometry with both their porosity ratios and pore sizes. The scutoid, which is a combination of triangular, pentagonal and hexagonal surfaces, has high pore size with 3025 µm for PLA, 3008 µm for ABS. However, pore size over 1500 µm is not recommended for bone substitutes, as it is a significant disadvantage in terms of mechanical strength [101]. This disadvantage can be overcome by using a smaller unit cell or by reducing the pore size with additional struts, but this results in low porosity.

FEA Analysis Results

Finite element analysis (FEA) was used to determine the strength properties of structures under load. Three different scaffold designs created in the dimensions of $20 \times 20 \times 20$ mm. The von Mises stress, displacement, shear force and bending moment values were obtained by applying the distributed force over the struts, fixed in all directions with the lower struts. The number of elements and nodes used in the analysis are given in Table 1.

FEA, which is made to verify the uniaxial compression test of models made of two different materials, which are considered ductile and isotropic, is critical in determining the density of energy required to change the shape of the material. When the FEA results obtained in Fig. 7 are examined, the geometry with the highest strain resistance was determined as PLA printed cubic structure. The reason for this is that there are many vertical rods per unit element. It is seen that the material effect is low in the von Mises stresses in the cubic structure. It can be said that the use of PLA and ABS materials does not change the stresses.

In cubic structure, it is seen that the loads on the vertical axis accumulate in the cross-sections on the vertical axis (Fig. 7). In icosahedron structure, it is seen that the stresses change significantly with the use of ABS and PLA materials. Obtained reaction forces have very significant changes by geometries when the displacement value of 5 mm is applied. The model with the highest reaction forces emerges as cubic, icosahedron and scutoid structures, respectively. However, when the total displacement values were examined, it was observed that the highest values were 13.75 mm (for ABS P430) and 11.62 mm (for PLA) in the scutoid geometry due to the length of the vertical struts. The stress value obtained on the cubic scaffold produced with PLA material was 296.51 MPa. Due to the low amount of elastic elongation, while the stress values increase, it also causes the reaction force to be increased. Similarly, these results also show that the cubic geometry provides the highest strength 296.51 MPa (for ABS P430) and 191.68 MPa (for PLA) among the three scaffolds.

Shear stress is more of a geometry-related issue, it is difficult to say precisely because of the materials. When the buckling moment is examined, although the flexibility of the material is important, there is a geometry-induced change

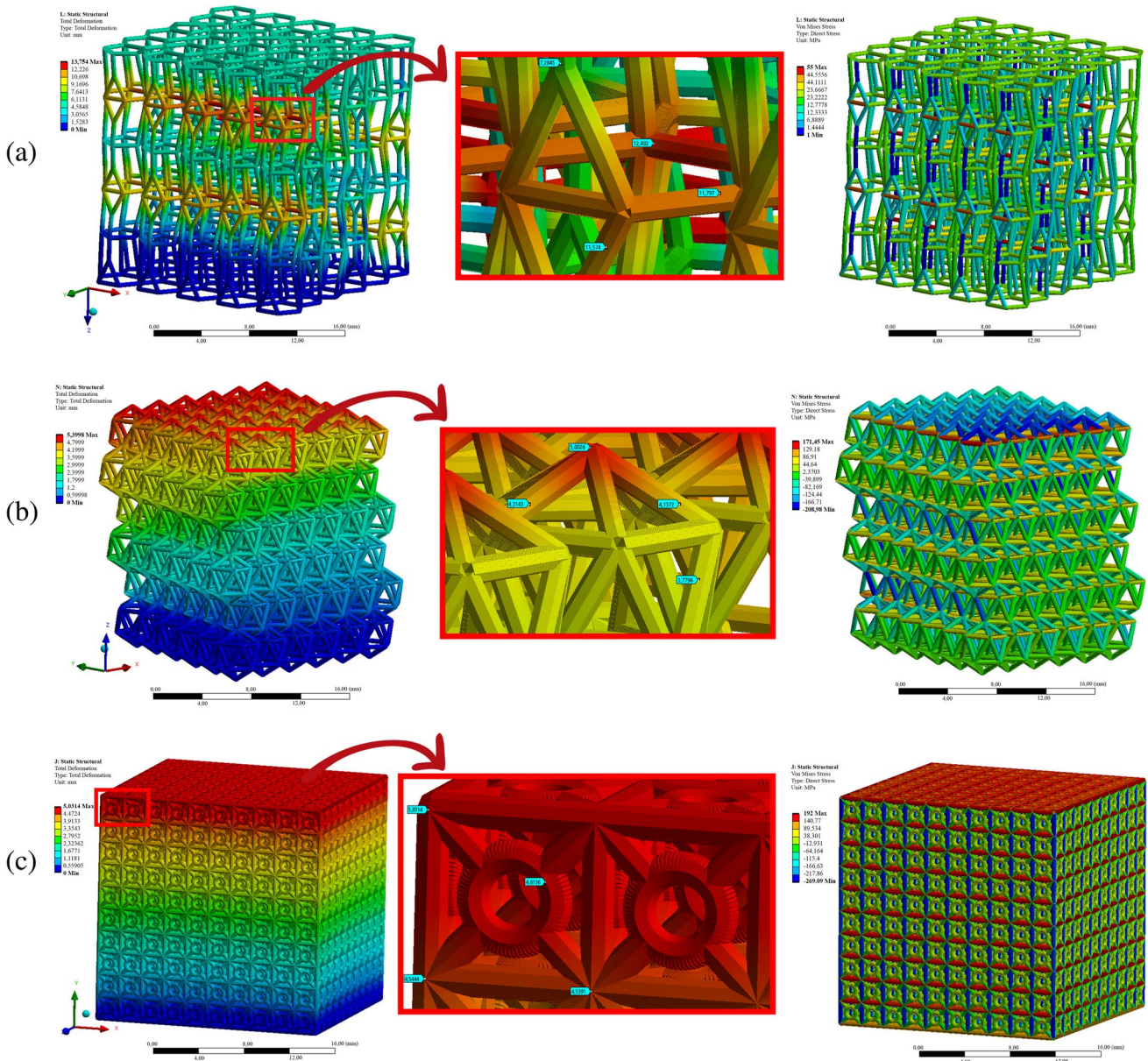


Fig. 7 Prediction of nonlinear compressive behavior of ABS P430 lattice structure using Newton–Raphson FEA results: (a) Scutoid, (b) Icosahedron, (c) Cubic

Table 5 Comparison of FEA results with ABS and PLA

Scaffolds		Reaction force [N]	Total displacement [mm]	Share force [N]	Bending moment [N.mm]	Von misses stress [MPa]
Cubic	ABS P430	25.102	5.03	55.69	32.85	191.68
Icosahedron		5.579	5.39	10.56	26.94	171.45
Scutoid		1.485	13.75	2.04	5.49	54.93
Cubic	PLA	29.412	4.27	47.33	29.33	296.51
Icosahedron		6.564	4.85	7.22	14.48	254.43
Scutoid		1.748	11.62	1.18	4.41	96.57

like the shear strength. Although there is no important difference between PLA and ABS material changes, it has been observed that there are significant changes due

to geometry. While the highest buckling moment and shear force occurred in cubic with 55 N and 32 N.mm, respectively, the lowest values also occurred in scutoid



regardless of the material. In Table 5, the FEA results were shown by comparing different materials and geometries.

Compression Test

In the compression test, 50 kN load was applied to the 3D printed structures in vertical direction with a speed of 5 mm/min. The deformation rate was determined as 0.0833 mm/sec in order to better observe the effect of the compression speed on the mechanical behavior of the scaffold geometries in the compression tests performed to determine the strength characteristics of the parts under load. Besides, rapid camera images were used to better observe the initiation and progress of deformation, so it was determined from which area the cells started to be crushed during the crushing.

As seen in Fig. 8, during the compression test, the deformation in the directions perpendicular to the compression direction is almost non-existent. For this reason, it has been determined that the Poisson ratio is approximately zero. In similar studies, it is stated that the Poisson ratio in plastic deformation is equal to zero. The permanent deformations that occur on the parts after the test.

According to the compression test results, it was observed that the cubic started to deform under 63.456 MPa, icosahedron is 7.519 MPa and scutoid scaffold is 2.276 MPa in produced with PLA material. Otherwise, it was observed that plastic deformation started under 75.54 MPa pressure in cubic, 6.0119 MPa in icosahedron and 1.765 MPa in scutoid scaffold produced with ABS material. It was observed that the maximum stress values of the structures without the cubic geometry produced with PLA material were higher. It has been evaluated that this situation is caused by the fact that the support material cannot be fully resolved in the cubic geometry, which has a low pore ratio compared to other geometries in the printings made with ABS material.

Elastic modulus (E) is calculated with equation (7) and shown in Table 6. Accordingly, the highest elastic modulus value was seen in cubic geometries in prints made with both ABS and PLA materials.

$$E = \frac{\sigma}{\epsilon} \tag{7}$$

where, σ is compressive stress and ϵ is compressive strain. The reason why the elastic modulus of the scutoid geometry is higher than the icosahedron is because it has a much lower compressive strain value than the icosahedron, as can be seen from the stress–strain graphs given in Fig. 8.

When the mechanical strength behaviors obtained are examined, it is seen that all models provide sufficient elastic strength for the bone scaffold. When the results of shear stress are examined, it is evaluated that cubic and icosahedron models can show similar behavior not only in vertical loads,

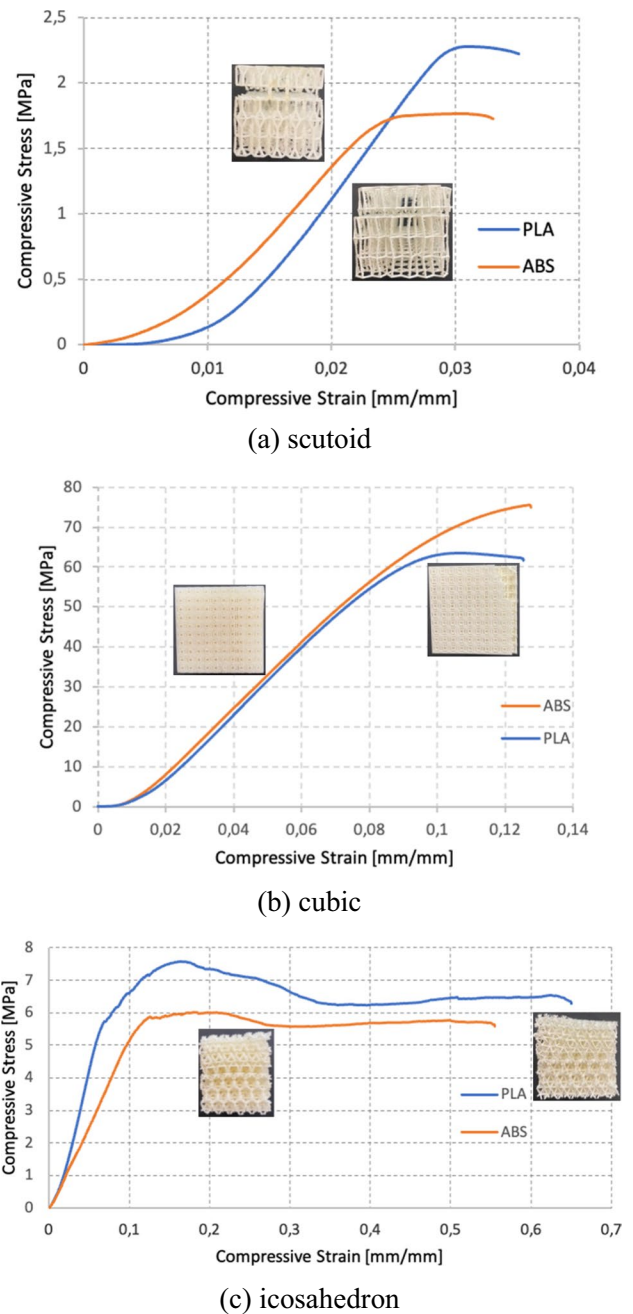


Fig. 8 Test results of test sample compression produced with PLA and ABS

Table 6 Elastic modulus of the scaffolds (MPa)

Scaffolds	PLA	ABS
Scutoid	72.9994171	58.5975377
Cubic	597.22792	593.01436
Icosahedron	42.4750115	32.8369567

but in all directions. Regardless of the material, the scutoid is the geometry with the highest elastic elongation. In cubic and icosahedron structures with high load strength, fracture behavior occurs from the length to the abrupt and at angles close to the vertical axis. On the other hand, in the scutoid, no fracture behavior was observed in the vertical axis, but a fracture parallel to the horizontal axis. As a result, it was determined that the scutoid should be positioned according to the expected load for the bone scaffold. The scutoid, which has the highest porosity ratio, is the weakest geometry in terms of elastic strength. This confirms that there is a close relationship between porosity rate and fracture behavior.

Conclusions

In this study, the bone scaffold production process with AM technologies, which are increasingly used due to the advantages they provide in BTE applications, is discussed. The aim of the study is to determine the effect of bio-inspired microstructures on dimensional accuracy, weight, mechanical performance, structural strength, porosity and pore size. The scaffold structures were printed with PLA and ABS-P430 filaments using FDM printers.

According to the results of the study, PLA scaffolds are more suitable than ABS in terms of dimensional accuracy. The strut diameters of PLA printed structures have a maximum deviation of 3.75% from the design diameter, and ABS printed structures have a maximum deviation of 5.25%. The lowest deviation rates were seen in PLA-printed icosahedron and cubic structures. On the other hand, the porosity of PLA printed scaffolds is higher than ABS printed scaffolds with the same design. The use of support materials in the printing of ABS scaffolds has reduced the porosity. While PLA printed scutoid geometry has the highest porosity with 94.7%, ABS printed cubic geometry has the lowest porosity with 55.9%. When the deviations in the porosity of CAD based and 3D printed scaffolds are examined, it is seen that PLA printed scaffolds have lower deviations. Besides, although the density of PLA is higher than ABS, the use of support material in ABS printed scaffolds increased the weight.

When the pore diameters of the 3D-printed scaffolds were examined, the pore sizes of PLA-printed cubic and icosahedron structures were determined as 411 μm and 722 μm , respectively. The pore sizes in ABS printed scaffolds were measured as 697 μm for the icosahedron and 405 μm for the cubic, respectively. Therefore, the results show that cubic and icosahedron structures can be used as scaffold geometry with both their porosity ratios and pore sizes. The scutoid geometry has a high pore size of 3025 μm for PLA and 3008 μm for ABS. However, pore size over 1500 μm is not recommended for bone scaffolds, as it is a significant disadvantage in terms of mechanical strength [101].

As a consequence, PLA printed scaffolds have better results than ABS printed scaffolds in terms of dimensional accuracy, porosity, pore diameter and weight. Among the PLA-printed scaffolds, the high pore diameter of the scutoid geometry resulted in low mechanical strength. In terms of porosity, the icosahedron geometry gave better results than the cubic structure. Therefore, PLA-printed icosahedron geometry can be considered as the most suitable scaffold type for bone tissue regeneration.

According to the compression test results, it was observed that the cubic started to deform under 63.456 MPa, icosahedron is 7.519 MPa and scutoid scaffold is 2.276 MPa in produced with PLA material. Otherwise, it was observed that plastic deformation started under 75.54 MPa pressure in cubic, 6.0119 MPa in icosahedron and 1.765 MPa in scutoid scaffold produced with ABS material. Maximum stress values were higher in geometries other than cubic geometry. The higher wear of stress values in cubic geometry is related to the presence of more cellular units in the scaffold structure due to the unit cell geometry. Even if the edge dimensions of the cellular units are taken equal for all geometries, the number of unit cells changed due to the geometry during the scaffolding process.

The main limitation of the study is that besides mechanical tests, biological experiments were not performed. Adding biological experiments to BTE applications better demonstrates the effect of pores on bone tissue regeneration [103–105]. Another limitation of this study is the dissolution process of the support material. The solution of support materials used for ABS printed scaffolds became more difficult as the pore size became smaller. Thus, insufficient dissolution of the support material affected the results in the mechanical strength tests. In future studies, methods that allow model production without using support materials can be used in the production of artificial bone scaffolds. Moreover, future studies will focus on studies that will determine the performance of the designed scaffold structures through biological experiments.

Acknowledgements All authors made contributions to the manuscript and have approved the final version of the script.

Author Contributions Neslihan Top: Writing—original draft (lead), design and modeling.

Harun Gökçe: Writing—review and editing, Mechanical and FEA tests.

İsmail Şahin—Writing—review and editing, Supervision (supporting).

Data Availability Statement The data that support the findings of this study are available from the corresponding author upon reasonable request.

Declarations

Declaration of Competing Interest The authors declare that they have no known competing financial interests or personal relationships that could have appeared to influence the work reported in this paper.

Conflicts of Interest The authors declare no conflicts of interest.



References

- Ghassemi T, Shahroodi A, Ebrahimzadeh MH, Mousavian A, Movaffagh J, Moradi A (2018) Current concepts in scaffolding for bone tissue engineering. *Arch Bone Joint Surg* 6(2):90
- Qu H (2020) Additive manufacturing for bone tissue engineering scaffolds. *Mater Today Commun* 24:101024
- Müller B, Deyhle H, Fierz F, Irsen S, Yoon J, Mushkolaj S, Boss O, Vondran E, Gbureck U, Degstrici Ö (2009) Biomimetic hollow scaffolds for long bone replacement. *Proc SPIE - Int Soc Opt Eng* 7401(1):1–13
- Top N, Şahin İ, Gökçe H (2019) Artificial bone scaffold design in tissue engineering. *Selcuk Tech J* 18(3):209–228
- Salgado AJ, Coutinho OP, Reis RL (2004) Bone tissue engineering: state of the art and future trends. *Macromol Sci* 4(8):743–765
- Rezwan K, Chen QZ, Blaker JJ, Boccaccini AR (2006) Biodegradable and bioactive porous polymer inorganic composite scaffolds for bone tissue engineering. *Biomaterials* 27(18):3413–3431
- Seitz H, Rieder W, Irsen S, Leukers B, Tille C (2005) Three-dimensional printing of porous ceramic scaffolds for bone tissue engineering. *J Biomed Mater Res B Appl Biomater* 74(2):782–788
- Li J, Chen M, Fan X, Zhou H (2016) Recent advances in bioprinting techniques: approaches, applications and future prospects. *J Transl Med* 14(1):271
- Guo Y, Liu K, Yu Z (2019) Tetrahedron based porous scaffold design for 3D printing. *Designs* 3(16):1–17
- O'Brien FJ (2011) Biomaterials & scaffolds for tissue engineering. *Mater Today* 14(3):88–95
- Habibovic P, Gbureck U, Doillon CJ, Bassett DC, Blitterswijk CAV, Barralet JE (2008) Osteoconduction and osteoinduction of low-temperature 3D printed bioceramic implants. *Biomaterials* 29(7):944–953
- Jones AC, Arns CH, Sheppard AP, Huttmacher DW, Milthorpe BK, Knackstedt MA (2007) Assessment of bone ingrowth into porous biomaterials using Micro-CT. *Biomaterials* 28(15):2491–2504
- Polo-Corrales L, Latorre-Estevés M, Ramirez-Vick JE (2014) Scaffold design for bone regeneration. *J Nanosci Nanotechnol* 14(1):15–56
- Gregor A, Filová E, Novák M, Kronek J, Chlup H, Buzgo M, Blahnová V, Lukášová V, Bartoš M, Nečas A, Hošek J (2017) Designing of PLA scaffolds for bone tissue replacement fabricated by ordinary commercial 3D printer. *J Biol Eng* 11(1):31
- Zaszczyńska A, Moczulska-Heljak M, Gradys A, Sajkiewicz P (2021) Advances in 3D printing for tissue engineering. *Materials* 14(12):3149
- Mota C, Puppi D, Chiellini F, Chiellini E (2015) Additive manufacturing techniques for the production of tissue engineering constructs. *J Tissue Eng Regen Med* 9(3):174–190
- Bose S, Suguira S, Bandyopadhyay A (1999) Processing of controlled porosity ceramic structures via fused deposition. *Scripta Mater* 41(9):1009–1014
- Gibson I, Rosen DW, Stucker B (2015) Additive manufacturing technologies. Springer, New York, 13:43
- Wang L, Kang J, Sun C, Li D, Cao Y, Jin Z (2017) Mapping porous microstructures to yield desired mechanical properties for application in 3D printed bone scaffolds and orthopaedic implants. *Mater Des* 133:62–68
- Santos ARC, Almeida HA, Bártolo PJ (2013) Additive manufacturing techniques for scaffold-based cartilage tissue engineering: a review on various additive manufacturing technologies in generating scaffolds for cartilage tissue engineering. *Virtual Phys Prototyp* 8(3):175–186
- Top N, Şahin İ, Gökçe H, Gökçe H (2021) Computer-aided design and additive manufacturing of bone scaffolds for tissue engineering: state of the art. *J Mater Res* 36(19):3725–3745
- Datta P, Vyas V, Dhara S, Chowdhury AR, Barui A (2019) Anisotropy properties of tissues: a basis for fabrication of biomimetic anisotropic scaffolds for tissue engineering. *J Bionic Eng* 16(5):842–868
- Yang Y, Song X, Li X, Chen Z, Zhou C, Zhou Q, Chen Y (2018) Recent progress in biomimetic additive manufacturing technology: from materials to functional structures. *Adv Mater* 30(36):1706539
- Smith MH, Flanagan CL, Kempainen JM, Sack JA, Chung H, Das S, ..., Feinberg SE (2007) Computed tomography-based tissue-engineered scaffolds in craniomaxillofacial surgery. *Int J Med Robot Comput Assisted Surg* 3(3): 207–216
- Sun W, Starly B, Nam J, Darling A (2005) Bio-CAD modeling and its applications in computer-aided tissue engineering. *Comput Aided Des* 37(11):1097–1114
- Chen G, Luo H, Zhang Z, Fan X (2020) Flexural deformation and fracture behaviors of the sandwich turtle rib bones with hierarchical woven fibers. *Colloid Interface Sci Commun* 34:100230
- Ott J, Lazalde M, Gu GX (2020) Algorithmic-driven design of shark denticle bioinspired structures for superior aerodynamic properties. *Bioinspir Biomim* 15(2):026001
- Ren L, Li B, Song Z, Liu Q, Ren L, Zhou X (2019) 3D printing of structural gradient soft actuators by variation of bioinspired architectures. *J Mater Sci* 54(8):6542–6551
- Ghazlan A, Ngo T, Nguyen T, Linforth S, Van Le T (2020) Uncovering a high-performance bio-mimetic cellular structure from trabecular bone. *Sci Rep* 10(1):1–13
- Ghazlan A, Nguyen T, Ngo T, Linforth S (2020) Performance of a 3D printed cellular structure inspired by bone. *Thin-Walled Struct* 151:106713
- Chen H, Han Q, Wang C, Liu Y, Chen B, Wang J (2020) Porous scaffold design for additive manufacturing in orthopedics: a review. *Front Bioeng Biotechnol* 8:609
- Yang Y, Wang G, Liang H, Gao C, Peng S, Shen L, Shuai C (2019) Additive manufacturing of bone scaffolds. *Int J Bioprint* 5(1):1–25
- Jiao C, Xie D, He Z, Liang H, Shen L, Yang Y, ..., Wang C (2022) Additive manufacturing of bio-inspired ceramic bone Scaffolds: structural design, mechanical properties and biocompatibility. *Mater Des* 217: 110610
- Liang H, Chao L, Xie D, Yang Y, Shi J, Zhang Y, ..., Jiang Q (2022) Trabecular-like Ti–6Al–4V scaffold for bone repair: A diversified mechanical stimulation environment for bone regeneration. *Compos Part B: Eng* 241:110057
- Krzysztof P, Pokrowiecki R (2018) Porous titanium implants: a review. *Adv Mater Eng* 20:1700648
- Nazir A, Abate KM, Kumar A, Jeng J-Y (2019) A state-of-the-art review on types, design, optimization, and additive manufacturing of cellular structures. *Int J Adv Manuf Technol* 104:3489–3510
- Savio G, Rosso S, Meneghello R, Concheri G (2018) Geometric modeling of cellular materials for additive manufacturing in biomedical field: a review. *Appl Bionics Biomech* 2018:1654782
- Du X, Fu S, Zhu Y (2018) 3D printing of ceramic-based scaffolds for bone tissue engineering: an overview. *J Mater Chem B* 6(27):4397–4412
- Nouri A, Shirvan AR, Li Y, Wen C (2021) Additive manufacturing of metallic and polymeric load-bearing biomaterials using laser powder bed fusion: a review. *J Mater Sci Technol* 94:196–215
- Liang H, Ji T, Zhang Y, Wang Y, Guo W (2017) Reconstruction with 3D-printed pelvic endoprostheses after resection of a pelvic tumour. *Bone Joint J* 99(2):267–275
- Phan K, Sgro A, Maharaj MM, D'Urso P, Mobbs RJ (2016) Application of a 3D custom printed patient specific spinal implant for C1/2 arthrodesis. *Journal of Spine Surgery* 2(4):314

42. Wang L, Cao T, Li X, Huang L (2016) Three-dimensional printing titanium ribs for complex reconstruction after extensive posterolateral chest wall resection in lung cancer. *J Thorac Cardiovasc Surg* 152(1):e5–e7
43. Chen Y, Li W, Zhang C, Wu Z, Liu J (2020) Recent developments of biomaterials for additive manufacturing of bone scaffolds. *Adv Healthc Mater* 9(23):2000724
44. Liu F, Wang X (2020) Synthetic polymers for organ 3D printing. *Polymers* 12(8):1765
45. Wang X, Liu C (2018). 3D Bioprinting of Adipose-Derived Stem Cells for Organ Manufacturing. In: Chun H, Park C, Kwon I, Khang G (eds) *Cutting-Edge Enabling Technologies for Regenerative Medicine. Advances in Experimental Medicine and Biology*, Springer, Singapore 3–14
46. Roseti L, Parisi V, Petretta M, Cavallo C, Desando G, Bartolotti I, Grigolo B (2017) Scaffolds for bone tissue engineering: state of the art and new perspectives. *Mater Sci Eng C* 78:1246–1262
47. Eltom A, Zhong G, & Muhammad A (2019) Scaffold techniques and designs in tissue engineering functions and purposes: a review. *Adv Mater Sci Eng* 2019:1–13
48. Baptista R, Guedes M (2021) Morphological and mechanical characterization of 3D printed PLA scaffolds with controlled porosity for trabecular bone tissue replacement. *Mater Sci Eng: Part C* 118:111528
49. Fairag R, Rosenzweig DH, Ramirez-Garcialuna JL, Weber MH, Haglund L (2019) Three-dimensional printed polylactic acid scaffolds promote bone-like matrix deposition in vitro. *ACS Appl Mater Interfaces* 11(17):15306–15315
50. Germain L, Fuentes CA, van Vuure AW, des Rieux A, Dupont-Gillain C (2018) 3D-printed biodegradable gyroid scaffolds for tissue engineering applications. *Mater Des* 151:113–122
51. Krishna LSR, Kamal M, Venkatesh S (2017) Design and manufacturing of a scaffold for biomedical applications using additive manufacturing. *Indian J Sci Res Dec.* 2017:1–7
52. Ariffin MKAM, Fazel SH, İsmail MIS, Mohamed S, Wahid Z (2018) Mechanical properties of bone scaffold prototypes fabricated by 3D printer. *J Eng Sci Technol* 13:29–38
53. Kantaros A, Chatzidai N, Karalekas D (2016) 3D printing-assisted design of scaffold structures. *Int J Adv Manuf Technol* 82(1–4):559–571
54. Rosenzweig DH, Carelli E, Steffen T, Jarzem P, Haglund L (2015) 3D-printed ABS and PLA scaffolds for cartilage and nucleus pulposus tissue regeneration. *Int J Mol Sci* 16(7):15118–15135
55. Liu H, Ahlinder A, Yassin MA, Finne-Wistrand A, Gasser TC (2020) Computational and experimental characterization of 3D-printed PCL structures toward the design of soft biological tissue scaffolds. *Mater Des* 188:108488
56. Patricio T, Domingos M, Gloria A, Bártolo P (2013) Characterisation of PCL and PCL/PLA scaffolds for tissue engineering. *Procedia Cirp* 5:110–114
57. Gao C, Deng Y, Feng P, Mao Z, Li P, Yang B, Peng S (2014) Current progress in bioactive ceramic scaffolds for bone repair and regeneration. *Int J Mol Sci* 15(3):4714–4732
58. Chen M, Le DQ, Kjems J, Bünger C, Lysdahl H (2015) Improvement of distribution and osteogenic differentiation of human mesenchymal stem cells by hyaluronic acid and β -tricalcium phosphate-coated polymeric scaffold in vitro. *BioRes Open Access* 4(1):363–373
59. Jaidev LR, Chatterjee K (2019) Surface functionalization of 3D printed polymer scaffolds to augment stem cell response. *Mater Des* 161(1):44–54
60. Szivek JA, Wojtanowski A, David G, Jordan S (2016) Stem cell infiltrated biomimetic inverse trabecular-patterned scaffolds accelerate bone growth during long segment repair in a sheep critical sized defect. 10th World Biomaterials Congress, Montréal, Canada
61. Touri M, Moztafzadeh F, Osman NAA, Dehghan MM, Mozafari M (2018) 3D-printed biphasic calcium phosphate scaffolds coated with an oxygen generating system for enhancing engineered tissue survival. *Mater Sci Eng C* 84:236–242
62. Bankole I, Oladapo S, Adeoye AOM, Zahedi SA (2018) 3D printing of bone scaffolds with hybrid biomaterials. *Compos B Eng* 158(1):428–436
63. Chen G, Chen N, Wang Q (2019) Fabrication and properties of poly (vinyl alcohol)/ β -tricalcium phosphate composite scaffolds via fused deposition modeling for bone tissue engineering. *Compos Sci Technol* 172:17–28
64. Felfel RM (2016) In vitro degradation and mechanical properties of poly-PLA-PCL copolymer unit cell scaffolds generated by two-photon poly marination. *Biomed Mater* 11:015011
65. Jiao Z, Luo B, Xiang S, Ma H, Yu Y, Yang W (2019) 3D printing of HA/PCL composite tissue engineering scaffolds. *Adv Ind Eng Polymer Res* 2(4):196–202
66. Sahmani S, Khandan A, Esmaili S, Saber-Samandari S, Nejad MG, Aghdam MM (2020) Calcium phosphate-PLA scaffolds fabricated by fused deposition modeling technique for bone tissue applications: fabrication, characterization and simulation. *Ceram Int* 46(2):2447–2456
67. Zhang H, Mao X, Zhao D, Jiang W, Du Z, Li Q, ..., Han D (2017) Three dimensional printed polylactic acid-hydroxyapatite composite scaffolds for prefabricating vascularized tissue engineered bone: an in vivo bioreactor model. *Sci Rep* 7(1): 1–13
68. Feng P, Wu P, Gao C, Yang Y, Guo W, Yang W, Shuai C (2018) A multimaterial scaffold with tunable properties: toward bone tissue repair. *Adv Sci* 5(6):1700817
69. Shuai C, Peng B, Feng P, Yu L, Lai R, Min A (2022) In situ synthesis of hydroxyapatite nanorods on graphene oxide nanosheets and their reinforcement in biopolymer scaffold. *J Adv Res* 35:13–24
70. Shuai C, Yang W, Feng P, Peng S, Pan H (2021) Accelerated degradation of HAP/PLLA bone scaffold by PGA blending facilitates bioactivity and osteoconductivity. *Bioactive Mater* 6(2):490–502
71. Weems AC, Pérez-Madrigal MM, Arno MC, Dove AP (2020) 3D printing for the clinic: examining contemporary polymeric biomaterials and their clinical utility. *Biomacromol* 21(3):1037–1059
72. Alam F, Varadarajan KM, Kumar S (2020) 3D printed polylactic acid nanocomposite scaffolds for tissue engineering applications. *Polym Testing* 81:106203
73. Grémare A, Guduric V, Bareille R, Heroguez V, Latour S, Heureux N, Nihouannen D (2018) Characterization of printed PLA scaffolds for bone tissue engineering. *J Biomed Mater Res Part A* 106(4):887–894
74. Yeh CH, Chen YW, Shie MY, Fang HY (2015) Poly dopamine assisted immobilization of Xu Duan on 3D printed poly lactic acid scaffolds to up regulate osteogenic and angiogenic markers of bone marrow stem cells. *Materials* 8:4299–4315
75. de la Lastra A, Hixon K, Aryan L, Banks A, Lin A, Hall A, Sell S (2018) Tissue engineering scaffolds fabricated in dissolvable 3D printed molds for patient specific craniofacial bone regeneration. *J Funct Biomater* 9(3):46
76. Macdonald NP, Zhu F, Hall CJ, Reboud J, Crosier PS, Patton EE, Wlodkowic D, Cooper JM (2016) Assessment of biocompatibility of 3D printed photopolymers using zebrafish embryo toxicity assays. *Lab Chip* 16(2):291–297
77. Jo MY, Ryu YJ, Ko JH, Yoon JS (2012) Effects of compatibilizers on the mechanical properties of ABS/PLA composites. *J Appl Polym Sci* 125(S2):E231–E238
78. Bijarimi M, Shahadah N, Ramli A, Nuridin S, Alhadadi W, Muzakkar MZ, Jaafar J (2020) Poly (Lactic Acid)(PLA)/

- acrylonitrile butadiene styrene (ABS) with graphene nanoplatelet (GNP) nanocomposites. *Indonesian J Chem* 20(2):276–281
79. Choe JJ, Lee JH, Yu JH, Yoon JS (2014) Mechanical properties of acrylonitrile–butadiene–styrene copolymer/poly (l-lactic acid) blends and their composites. *J Appl Polymer Sci* 131(11):40329
 80. Rigoussen A, Verge P, Raquez JM, Habibi Y, Dubois P (2017) In-depth investigation on the effect and role of cardanol in the compatibilization of PLA/ABS immiscible blends by reactive extrusion. *Eur Polymer J* 93:272–283
 81. Elsharkawy S, Mata A (2018) Hierarchical biomineralization: from nature’s designs to synthetic materials for regenerative medicine and dentistry. *Adv Healthc Mater* 7(18):1800178
 82. Gómez S, Vlad MD, López J, Fernández E (2016) Design and properties of 3D scaffolds for bone tissue engineering. *Acta Biomater* 42:341–350
 83. Lv Y, Wang B, Liu G, Tang Y, Lu E, Xie K, ..., Wang L (2021) Metal material, properties and design methods of porous biomedical scaffolds for additive manufacturing: a review. *Front Bioeng Biotechnol* 9: 641130
 84. Hollister SJ (2005) Porous scaffold design for tissue engineering. *Nat Mater* 4(7):518–524
 85. Qi F, Gao X, Wang C, Shuai Y, Yang L, Liao R, ..., Shuai C (2022a) In situ grown silver nanoparticles on tetrapod-like zinc oxide whisker for photocatalytic antibacterial in scaffolds. *Mater Today Sustain* 19: 100210
 86. Qi F, Wang Z, Shuai Y, Peng S, Shuai C (2022) Sr²⁺ sustained release system augments bioactivity of polymer scaffold. *ACS Appl Polymer Mater* 4(4):2691–2702
 87. Shuai C, Liu G, Yang Y, Qi F, Peng S, Yang W, ..., Qian G (2020) A strawberry-like Ag-decorated barium titanate enhances piezoelectric and antibacterial activities of polymer scaffold. *Nano Energy* 74: 104825
 88. Han S, Currier T, Edraki M, Liu B, Lynch ME, Modarres-Sadeghi Y (2021) Flow inside a bone scaffold: Visualization using 3D phase contrast MRI and comparison with numerical simulations. *J Biomech* 126:110625
 89. Giannitelli SM, Accoto D, Trombetta M, Rainer A (2014) Current trends in the design of scaffolds for computer aided tissue engineering. *Acta Biomater* 10(2):580–594
 90. Liebschner MAK (2012) *Computer aided tissue engineering*, 1st Edn. Springer Humana
 91. Gómez-Gálvez P, Vicente-Munuera P, Tagua A, Forja C, Castro AM, Letrán M, ..., Escudero LM (2018) Scutoids are a geometrical solution to three-dimensional packing of epithelia. *Nat Commun* 9(1): 1–14
 92. Top N (2019) Design and production of a novel bone scaffolding using additive manufacturing for tissue engineering, MSc Thesis, Gazi University, Graduate School of Natural and Applied Sciences, Ankara, Turkey
 93. Egan PF, Gonella VC, Engelsperger M, Ferguson SJ, Shea K (2017) Computationally designed lattices with tuned properties for tissue engineering using 3D printing. *PLoS One* 12(8):e0182902
 94. Esslinger S, Gadow R (2020) Additive manufacturing of bioceramic scaffolds by combination of FDM and slip casting. *J Eur Ceram Soc* 40(11):3707–3713
 95. Arabnejad S, Johnston RB, Pura JA, Singh B, Tanzer M et al (2016) High-strength porous biomaterials for bone replacement: a strategy to assess the interplay between cell morphology, mechanical properties, bone ingrowth and manufacturing constraints. *Acta Biomater* 30:345–356
 96. Lemons JE (1987) Quantitative characterization and performance of porous implants for hard tissue applications: a symposium, ASTM international
 97. Karageorgiou V, Kaplan D (2005) Porosity of 3D biomaterial scaffolds and osteogenesis. *Biomaterials* 26(27):5474–5491
 98. Roosa SMM, Kempainen JM, Moffitt EN, Krebsbach PH, Hollister SJ (2010) The pore size of polycaprolactone scaffolds has limited influence on bone regeneration in an in vivo model. *J Biomed Mater Res Part A* 92(1):359–368
 99. Abbasi N, Hamlet S, Love RM, Nguyen NT (2020) Porous scaffolds for bone regeneration. *J Sci: Adv Mater Devices* 5(1):1–9
 100. Bragdon CR, Jasty M, Greene M, Rubash HE, Harris WH (2004) Biologic fixation of total hip implants: Insights gained from a series of canine studies. *JBJS* 86:105–117
 101. Ghayor C, Weber FE (2018) Osteoconductive microarchitecture of bone substitutes for bone regeneration revisited. *Front Physiol* 9:960
 102. Dias MR, Fernandes PR, Guedes JM, Hollister SJ (2012) Permeability analysis of scaffolds for bone tissue engineering. *J Biomech* 45(6):938–944
 103. Feng P, Jia J, Peng S, Shuai Y, Pan H, Bai X, Shuai C (2022) Transcrystalline growth of PLLA on carbon fiber grafted with nano-SiO₂ towards boosting interfacial bonding in bone scaffold. *Biomater Res* 26(1):1–15
 104. Feng P, Shen S, Yang L, Kong Y, Yang S, Shuai C (2023) Vertical and uniform growth of MoS₂ nanosheets on GO nanosheets for efficient mechanical reinforcement in polymer scaffold. *Virtual Phys Prototyp* 18(1):e2115384
 105. Feng P, Wang K, Shuai Y, Peng S, Hu Y, Shuai C (2022) Hydroxyapatite nanoparticles in situ grown on carbon nanotube as a reinforcement for poly (ϵ -caprolactone) bone scaffold. *Mater Today Adv* 15:100272

Publisher's Note Springer Nature remains neutral with regard to jurisdictional claims in published maps and institutional affiliations.

Springer Nature or its licensor (e.g. a society or other partner) holds exclusive rights to this article under a publishing agreement with the author(s) or other rightsholder(s); author self-archiving of the accepted manuscript version of this article is solely governed by the terms of such publishing agreement and applicable law.

